Title

Quantum Mechanical Screening of Single-Atom Bimetallic Alloys for the Selective Reduction of CO2 to C1 Hydrocarbons

Journal

ACS Catalysis, 6(11)

ISSN

2155-5435

Authors

Cheng, Mu-Jeng
Clark, Ezra L
Pham, Hieu H
et al.

Publication Date

2016-11-04

DOI

10.1021/acscatal.6b01393

Peer reviewed

ACS Catalysis

Research Article

pubs.acs.org/acscatalysis

Quantum Mechanical Screening of Single-Atom Bimetallic Alloys for the Selective Reduction of CO_2 to C_1 Hydrocarbons

Mu-Jeng Cheng,[†,‡] Ezra L. Clark,[†,§] Hieu H. Pham,[†] Alexis T. Bell,[*,†,§] and Martin Head-Gordon[*,†,‡]

[†]The Joint Center for Artificial Photosynthesis, Lawrence Berkeley National Laboratory, Berkeley, California 94720, United States

[‡]Department of Chemistry, University of California at Berkeley, Berkeley, California 94720, United States

[§]Department of Chemical and Biomolecular Engineering, University of California at Berkeley, Berkeley, California 94720, United States

Supporting Information

ABSTRACT: Electrocatalytic reduction of CO_2 to energy-rich hydrocarbons such as alkanes, alkenes, and alcohols is a very challenging task. So far, only copper has proven to be capable of such a conversion. We report density functional theory (DFT) calculations combined with the Poisson−Boltzmann implicit solvation model to show that single-atom alloys (SAAs) are promising electrocatalysts for CO_2 reduction to C_1 hydrocarbons in aqueous solution. The majority component of the SAAs studied is either gold or silver, in combination with isolated single atoms, M (M = Cu, Ni, Pd, Pt, Co, Rh, and Ir), replacing surface atoms. We envision that the SAA behaves as a one-pot tandem catalyst: first gold (or silver) reduces CO_2 to CO, and the newly formed CO is then captured by M and is further reduced to C_1 hydrocarbons such as methane or methanol. We studied 28 SAAs, and found about half of them selectively favor the CO_2 reduction reaction over the competing hydrogen evolution reaction. Most of those promising SAAs contain M = Co, Rh, or Ir. The reaction mechanism of two SAAs, Rh@Au(100) and Rh@Ag(100), is explored in detail. Both of them reduce CO_2 to methane but via different pathways. For Rh@Au(100), reduction occurs through the pathway *CO → *CHO → *CHOH → *CH + $H_2O_{(l)}$ → *CH_2 + $H_2O_{(l)}$ → *CH_3 + $H_2O_{(l)}$ → * + $H_2O_{(l)}$ + $CH_{4(g)}$; whereas, for Rh@Ag(100), the pathway is *CO → *CHO → *CH_2O→ *OCH_3 → *O + $CH_{4(g)}$ → *OH + $CH_{4(g)}$ → * + $H_2O_{(l)}$ + $CH_{4(g)}$. The minimum applied voltages to drive the two electrocatalytic systems are −1.01 and −1.12 V_{RHE} for Rh@Au(100) and Rh@Ag(100), respectively, at which the Faradaic efficiencies for CO_2 reduction to CO are 60% for gold and 90% for silver. This suggests that SAA can efficiently reduce CO_2 to methane with as small as 40% loss to the hydrogen evolution reaction for Rh@Au(100) and as small as 10% for Rh@Ag(100). We hope these computational results can stimulate experimental efforts to explore the use of SAA to catalyze CO_2 electrochemical reduction to hydrocarbons.

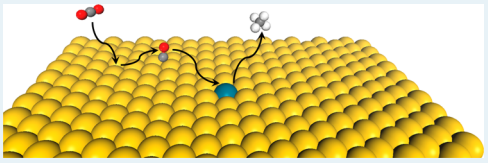

KEYWORDS: *CO_2 reduction, single-atom alloys, one-pot tandem catalyst, electrocatalysis, density functional theory*

1. INTRODUCTION

Global energy consumption is projected to triple by the end of the 21st century, relative to the present rate, because of population and economic growth.[1,2] While this increased energy demand can be met through the use of fossil fuels (petroleum and coal), doing so is expected to triple the level of atmospheric CO_2 by the end of the century.[1] Such a dramatic increase in atmospheric CO_2 concentration in the atmosphere is likely to perturb global ecosystems on an unprecedented scale.[3] A potential means for reducing CO_2 concentration and achieving carbon neutrality is the electrochemical reduction of CO_2 to fuel using electricity produced from wind, solar radiation, and geothermal heat. To achieve this goal, it is necessary to discover electrocatalysts for CO_2 reduction that are inexpensive (ideally composed of Earth-abundant materials), efficient (having low overpotentials), selective, and stable.[4−13] With regard to selectivity, the objective is to obtain high Faradaic efficiencies to the products of CO_2 reduction while reducing the Faradaic efficiency for the hydrogen evolution reaction (HER), which can dominate, particularly at less negative applied voltages.[14−18]

In thermodynamic terms, the outcome of the electrocatalysis is determined by the stability of the first hydrogenation intermediates (*COOH or *OCHO for CO_2RR, and *H for HER; see Scheme 1).[19−21] If *COOH or *OCHO is more stable than *H, it will occupy the active sites, and then the CO_2RR is the primary pathway; on the other hand, if *H is more stable, then the HER will be the dominant pathway. Since the formation of these intermediates all involve the transfer of one (H^+ + e^-) pair, variations in the applied voltage (assuming the interaction between the dipole of the adsorbate and the space-charge field is small and can be ignored)[22] or pH will not affect the relative stability of the *COOH, *OCHO, or *H intermediates. As a consequence, the key to enhancing the CO_2RR and to suppressing the HER is discovery of

Received: May 18, 2016
Revised: September 19, 2016
Published: September 23, 2016

DOI: 10.1021/acscatal.6b01393
ACS Catal. 2016, 6, 7769−7777

Scheme 1. Schematic Description of the First Two Hydrogenation Steps for the Electrochemical CO_2 Reduction Reaction and Hydrogen Evolution Reaction[a]

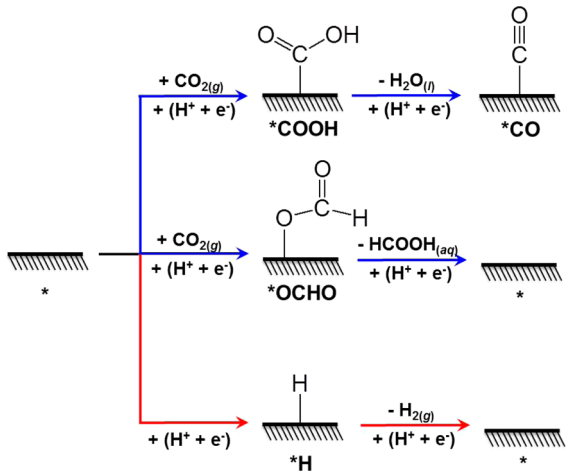

[a]The asterisk symbol (*) represents the surface, and "*A" represents A adsorbed on the surface.

electrocatalysts that bind *COOH or *OCHO more strongly than *H (ΔG_{*COOH} or $\Delta G_{*OCHO} < \Delta G_{*H}$, where ΔG_{*COOH}, ΔG_{*OCHO}, and ΔG_{*H} are the Gibbs free energies of formation for surface-bonded COOH, OCHO, and H species, respectively, referenced to a clean surface, $H_{2(g)}$, and $CO_{2(g)}$).

Meeting this criterion has proven to be a very challenging task. Karamad et al. have used density functional theory (DFT) to predict the performance of 34 intermetallic alloys for CO_2RR, relative to that for HER.[20] They found that ΔG_{*COOH} (or ΔG_{*OCHO}) > ΔG_{*H} for all 34 materials, meaning that HER would be the dominant reaction pathway in all cases. Changing the electrocatalysis to consider the competition between the CO reduction reaction (CORR) versus HER on the same 34 catalysts showed that four of them can perform CORR preferentially to HER. In other words, four cases satisfy ΔG_{*CHO} (or ΔG_{*COH}) < ΔG_{*H}, where *CHO and *COH are the first hydrogenated intermediates of CORR (see Scheme 2), and ΔG_{*CHO}, ΔG_{*COH}, and ΔG_{*H} are their Gibbs free energies of formation, relative to a clean surface, and $H_{2(g)}$, and $CO_{(g)}$.[20] Based on those discoveries, the authors proposed a two-pot tandem reaction for CO_2RR, in which CO_2 is first reduced to CO by well-defined existing protocols such as the reverse

Scheme 2. Schematic Description of the First Hydrogenation Step for the Electrochemical CO Reduction Reaction and Hydrogen Evolution Reaction

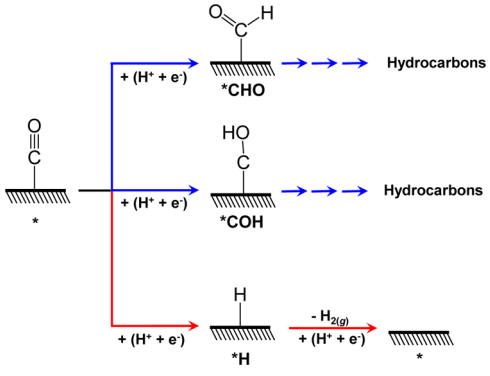

water–gas shift reaction,[23] and then CO is further reduced to hydrocarbons by those alloys. However, the capital cost for the proposed two-pot process is expected to be higher than that for an integrated system. Therefore, there is an opportunity to explore new types of electrochemical catalysts that can first convert CO_2 to CO, and then to hydrocarbons, while suppressing the HER.

In this study, quantum mechanical DFT calculations are used to screen 28 single-atom alloys (SAAs) as novel electrochemical catalysts for CO_2RR. Those catalysts are composed of isolated single atoms, M (M = Cu, Ni, Pd, Pt, Co, Rh, and Ir), embedded into the (111) and (100) surfaces of Au or Ag (Figure 1). The total number of SAAs is 28 ($7 \times 2 \times 2 = 28$), and we will denote these catalysts as M@Au(111), M@Au(100), M@Ag(111), or M@Ag(100).

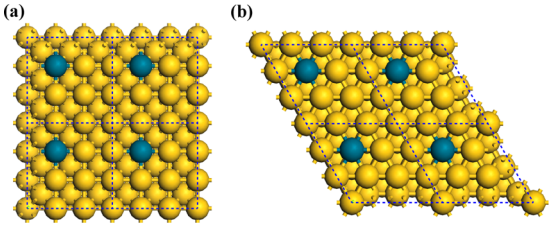

Figure 1. Surface models used to simulate the single-atom alloys: (a) M@Au(111), M@Ag(111), and (b) M@Au(100), M@Ag(100). Each model is composed of a three-layer slab, using a 3 × 3 periodic cell, where one Au or Ag atom on the topmost layer is replaced by M (M = Cu, Ni, Pd, Pt, Co, Rh, and Ir). This means that the doping concentration in the top layer is 11.1% (1/9). The periodic boundary is represented by the black dotted line.

Au and Ag are known for their ability to reduce CO_2 to CO with high Faradaic efficiencies,[17,18,24−28] in preference to the HER, and are the major component of our proposed catalysts. Therefore, we expect that CO_2 will first be selectively reduced to CO by the surrounding Au or Ag (Scheme 3). While Ag and

Scheme 3. Schematic Description of Our Proposed One-Pot Tandem Catalytic Reaction[a]

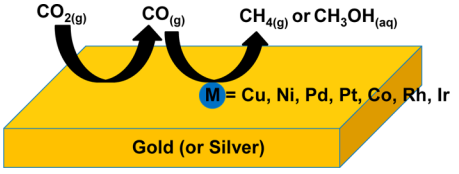

[a]The proposed electrocatalyst is composed primarily of gold or silver (colored gold), alloyed with small amounts of M (M = Cu, Ni, Pd, Pt, Co, Rh, and Ir). The feedstock CO_2 is first reduced to CO by gold or silver, and is subsequently captured and further reduced to C_1 products by M.

Au cannot further reduce CO, because of its much stronger binding interaction with M than with Au or Ag,[29] the newly formed CO will be preferentially bound to the single atom alloy site, M. There CO may be further reduced to hydrocarbons, if the CORR can be favored versus HER.

There are at least two advantages for this type of catalyst. First, since CO_2 reduction to CO, and the further reduction of CO to hydrocarbons are catalyzed by the same catalyst (the one-pot tandem catalyst), these SAAs are intrinsically simpler than a two-pot tandem approach, such as the one proposed by

DOI: 10.1021/acscatal.6b01393
ACS Catal. 2016, 6, 7769−7777

Karamad et al.[20] Second, because individual M atoms can accommodate only a single CO, and are isolated from each other by gold or silver, C−C coupling is unlikely. Therefore, the catalyst is expected to be selective for C_1 hydrocarbons (such as CH_4 and CH_3OH), and may even be selective for a single C_1 product, simplifying the challenge of product separation.

While our work is entirely computational, there are encouraging experimental precedents for the use of SAAs to catalyze a variety of chemical reactions, such as the electrochemical reduction of O_2 to H_2O_2, the selective hydrogenation of organic compounds, and the Ullmann reaction of aryl halides.[30−39] For example, Jirkovsky et al. have synthesized Pd@Au SAA and used it for selective reduction of O_2 to H_2O_2 with ∼95% selectivity.[38] Sykes and co-workers have synthesized Pd@Cu for the selective hydrogenation of styrene and acetylene[36] and Pt@Cu for 1,3-butadiene hydrogenation to butenes.[34] Also, Blaylock et al. have found Pd@Ag to be an efficient catalyst for the selective hydrogenation of acetylene and acrolein.[39]

The remainder of this paper is organized as follows. In Section 2, the computational approach that we employ is described. Our results are presented in Section 3, beginning with computational screening of 14 Au-based SAAs and 14 Ag-based SAAs, searching for alloys that exhibit high selectivity for CORR versus HER, as well as a relatively low applied bias to enable the endergonic CORR to proceed past the critical first reduction step. We then turn to a detailed mechanistic examination of two of the most promising alloys, showing that both of them appear to be selective for methane formation (over both methanol and hydrogen), as well as a discussion of some of the considerations that are relevant to possible future experimental preparation and study of these alloys.

2. COMPUTATIONAL DETAILS

The revised PBE functional (RPBE)[40] and the projector augmented wave pseudo-potentials,[41,42] as implemented in the Vienna ab initio Simulation Package (VASP),[43−46] were employed for all slab and molecule calculations. The Gaussian-smearing technique (smearing temperatures k_BT = 0.1 eV for slabs and 0.01 eV for molecules) was used to accelerate SCF convergence, after which all calculated values of energy were extrapolated to k_BT = 0. A Monkhorst−Pack k-point net of 3 × 3 × 1 was chosen to sample the reciprocal space for the slab calculations, whereas only the gamma point was sampled for the molecule calculations. Test calculations (see Computational Details in the Supporting Information) indicated that a 2 × 2 × 1 Monkhorst−Pack k-point net yields chemically significant changes in binding energy (as large as 0.22 eV for ΔG_{*COH}), while the changes upon extension to 5 × 5 × 1 are at least two times smaller. Extending the slab from three layers to four layers also yields similar energy changes of no more than ∼0.1 eV (see the Supporting Information), which are likely to be similar to inherent errors in the density functional itself.

To prevent interactions between the periodic replicas along the z-direction, a vacuum separation of at least 15 Å between adjacent images was used for the slab calculations, and a 20 Å × 20 Å × 20 Å box was used for molecular calculations. Spin-polarized wave functions were used for all surface calculations, while spin-restricted wave functions were used for molecular calculations. A dipole correction was not employed in this study, since test calculations showed that it has an insignificant effect on the binding energies of ΔG_{*H}, ΔG_{*CHO}, and ΔG_{*COH}.

As already shown in Figure 1, the slab models for all SAAs were composed of three metal layers, where each layer contains a 3 × 3 periodic cell. One Au or Ag atom on the topmost layer is substituted by M, leading to a surface substituent concentration of 1/9 (or 11.1%). During the geometry optimization, the atoms on the bottom layer were fixed in their bulk positions (a separation of 4.073 Å for Au, and 4.086 Å for Ag), whereas the atoms on the two top layers and all adsorbate atoms were allowed to relax. Geometries were optimized in water, simulated using the Poisson−Boltzmann implicit solvation model with a dielectric constant of ε = 80.[47]

All energies discussed in this work are free energies. For slabs, they were calculated as

$$G_{298K} = E_{elec}^{solv} + ZPVE + \sum_{\nu} \frac{h\nu}{e^{h\nu/kT} - 1} - T \times S_{vib}$$

The vibrational frequencies were evaluated for only surface adsorbates and were calculated by evaluating the partial Hessian matrix by finite differences. Based on the calculated vibrational frequencies, the zero-point vibrational energy (ZPVE), and vibrational contributions to the internal energy and entropy at 25 °C were calculated. The free energy of molecules was evaluated as

$$G_{298K} = E_{elec}^{solv} + ZPVE + \sum_{\nu} \frac{h\nu}{e^{h\nu/kT} - 1} + \left(\frac{n}{2}\right)kT - T(S_{vib} + S_{rot} + S_{trans})$$

where n = 8 for nonlinear molecules and n = 7 for linear molecules. E_{elec}^{solv} was obtained using the same approach as that for the slab systems. However, the ZPVE, the vibrational component of internal energy, and S_{vib}, S_{rot}, and S_{trans} were calculated by the Q-Chem package, using the same functional with the 6-31G* Gaussian-type basis set. Finally, it is well-known that gas-phase thermochemical reaction energies computed with the RPBE functional exhibit systematic deviations with experimental data.[48] Therefore, following previous theoretical work, a sensitivity analysis was performed for 21 chemical reactions,[49] and we found that a +0.38 eV correction for the electronic energy for CO_2 is needed.

For the investigation of reaction mechanisms, we assumed that proton and electron transfer are coupled. We also assumed that the barriers for hydrogenation through electrochemical means are small and easily surmountable at room temperature; therefore, we only considered thermodynamics and ignored kinetics. This assumption is supported by recent theoretical work showing the kinetic barriers are small, particularly under the influence of the applied voltages.[50] To relate our calculated free-energy diagrams at U = 0.0 V_{RHE} to different applied voltages, the computational hydrogen electrode (CHE) model proposed by Nørskov and co-workers was used.[51] In the CHE, the zero of voltage is defined to correspond to a proton and an electron in equilibrium with $H_{2(g)}$ at a pressure of 101 325 Pa. Using the standard relation between applied bias and free energy, the chemical potential of the proton and the electron at an applied bias (U) may then be expressed as $\mu(H^+) + \mu(e^-) = {}^1/_2\mu(H_{2(g)}) - eU$, where e is the electron charge.

To evaluate the performance of the DFT methods, we first calculated the equilibrium potentials for CO_2 reduction to formic acid, CO, formaldehyde, methanol, and methane (Table

DOI: 10.1021/acscatal.6b01393
ACS Catal. 2016, 6, 7769−7777

1), all of which are common intermediates during the reduction. As shown in Table 1, the equilibrium potentials

Table 1. Experimental[52] and Calculated Equilibrium Potential for Some Two-, Four-, Six-, and Eight-Electron Reductions

	reaction	Equilibrium Potential, U (eV, vs RHE) experiment	theory
1	$CO_{2(g)} + 2(H^+ + e^-) \rightarrow HCOOH_{(aq)}$	−0.20	−0.22
2	$CO_{2(g)} + 2(H^+ + e^-) \rightarrow CO_{(g)} + H_2O_{(l)}$	−0.12	−0.11
3	$CO_{2(g)} + 4(H^+ + e^-) \rightarrow CH_2O_{(aq)} + H_2O_{(l)}$	−0.07	−0.09
4	$CO_{2(g)} + 6(H^+ + e^-) \rightarrow CH_3OH_{(aq)} + H_2O_{(l)}$	0.03	0.03
5	$CO_{2(g)} + 8(H^+ + e^-) \rightarrow CH_{4(G)} + 2H_2O_{(l)}$	0.17	0.17

were calculated to be −0.22, −0.11, −0.09, 0.03, and 0.17 V_{RHE} for the reduction to formic acid, CO, formaldehyde, methanol, and methane, respectively. [Note: V_{RHE} is the unit of applied voltage (vs RHE).] Those numbers are in excellent agreement with the experimental values of −0.20, −0.12, −0.07, 0.03, and 0.17 V_{RHE}, respectively.[52]

3. RESULTS AND DISCUSSION

3.1. Identification of Catalysts with a High Selectivity to CORR. As stated in the Introduction, the requirement for a catalyst to be selective for CORR over HER is that either $\Delta G_{*CHO} < \Delta G_{*H}$ or $\Delta G_{*COH} < \Delta G_{*H}$, meaning that the catalyst binds with *CHO or *COH more tightly than with *H. Therefore, as the first step in our investigation, ΔG_{*CHO}, ΔG_{*COH}, and ΔG_{*H} were calculated for all 28 SAAs and the corresponding applied voltages needed to hydrogenate *CO to *CHO and *COH were evaluated. We considered all possible adsorption sites; however, the values of ΔG_{*CHO}, ΔG_{*COH}, and ΔG_{*H} reported in Table 2 are based on the most stable binding site (see Tables S1 and S2 in the Supporting Information).

Analyzing the results, we found that there are 10 alloys that favor CORR via the *CHO intermediate (i.e., $\Delta G_{*CHO} < \Delta G_{*H}$): Co@Au(111), Rh@Au(111), Ir@Au(111), Pt@Au(100), Rh@Au(100), Rh@Ag(111), Ir@Ag(111), Pt@Ag(100), Rh@Ag(100), and Ir@Ag(100). Three alloys favor CORR via the *COH intermediate (i.e., $\Delta G_{*COH} < \Delta G_{*H}$): Co@Au(100), Co@Ag(111), and Co@Ag(100). For Ir@Au(100), ΔG_{*CHO} and ΔG_{*COH} are the same, and both of them are smaller than ΔG_{*H}. Two interesting trends are observed. First, most of the alloys (except Pt@Au(100) and Pt@Ag(100)) that favor CORR have M = Co, Rh, and Ir. This means that choosing group 9 transition metals as M effectively enhances CO reduction and suppresses HER. Second, for most of the 28 SAAs (except Co@Au(100), Co@Ag(111), and Co@Ag(100)), *CHO is more stable than *COH. This means that *CO → *CHO is the most energetically favorable hydrogenation pathway for *CO, similar to what was observed in the Cu(211) system.[49]

Also, it should be mentioned that very recent theoretical studies using the surface charging technique to simulate the applied voltage show that the binding energy of *OCHO is voltage-dependent, although the variation is small.[53,54] It is possible that the binding energies of *H, *CHO, and *COH may also be slightly potential-dependent. This effect may affect our results for Ir@Au(111), Pt@Au(100), and Pt@Ag(100), since the values of ΔG_{*CHO} for these catalysts are only slightly smaller than that of ΔG_{*H} (by 0.06, 0.07, and 0.09 eV, respectively), and the stability of *CHO and *H could consequently be reversed for very negative applied voltages (e.g., −1.0 V_{SHE}).

Table 2. Calculated Binding Free Energy of *CHO (ΔG_{*CHO}), *COH (ΔG_{*COH}), and *H (ΔG_{*H}), and the Applied Bias Necessary for the Reduction of *CO to *CHO (U_{*CHO}) and *COH (U_{*COH})

catalyst	ΔG_{*H} (eV)	ΔG_{*CHO} (eV)	ΔG_{*COH} (eV)	U_{*CHO} (V_{RHE})	U_{*COH} (V_{RHE})
Cu@Au(111)	0.37	0.73	1.22	−0.61	−1.10
Ni@Au(111)	0.29	0.46	0.70	−1.10	−1.33
Pd@Au(111)	0.38	0.52	1.06	−0.69	−1.23
Pt@Au(111)	0.00	0.04	0.70	−0.70	−1.35
Co@Au(111)	0.14	−0.04	0.02	−1.21	−1.27
Rh@Au(111)	−0.10	−0.32	0.22	−0.96	−1.50
Ir@Au(111)	−0.50	−0.56	−0.37	−1.19	−1.39
Cu@Au(100)	0.23	0.64	1.34	−0.75	−1.44
Ni@Au(100)	0.01	0.20	0.36	−1.11	−1.27
Pd@Au(100)	0.09	0.24	0.89	−0.69	−1.34
Pt@Au(100)	−0.14	−0.21	0.20	−0.75	−1.16
Co@Au(100)	−0.12	−0.20	−0.36	−1.23	−1.08
Rh@Au(100)	−0.22	−0.46	−0.34	−1.01	−1.13
Ir@Au(100)	−0.57	−0.73	−0.73	−1.22	−1.22
Cu@Ag(111)	0.30	0.84	1.44	−0.81	−1.42
Ni@Ag(111)	0.02	0.18	0.74	−1.18	−1.74
Pd@Ag(111)	0.24	0.50	1.44	−0.80	−1.74
Pt@Ag(111)	−0.14	−0.06	0.93	−0.71	−1.70
Co@Ag(111)	−0.10	[a]	−0.23	[a]	−1.50
Rh@Ag(111)	−0.12	−0.36	0.23	−1.14	−1.73
Ir@Ag(111)	−0.56	−0.71	−0.36	−1.28	−1.63
Cu@Ag(100)	0.31	0.77	1.69	−0.88	−1.80
Ni@Ag(100)	−0.08	−0.03	0.54	−1.26	−1.82
Pd@Ag(100)	0.10	0.25	1.22	−0.87	−1.84
Pt@Ag(100)	−0.15	−0.24	0.78	−0.83	−1.84
Co@Ag(100)	−0.26	[a]	−0.41	[a]	−1.44
Rh@Ag(100)	−0.27	−0.59	−0.11	−1.12	−1.60
Ir@Ag(100)	−0.63	−0.89	−0.63	−1.26	−1.52

[a]Geometry optimization of *CHO leads to the formation of surface-bound H and CO species on Co.

DOI: 10.1021/acscatal.6b01393
ACS Catal. 2016, 6, 7769−7777

To understand the reason why alloys with M = Co, Rh, and Ir favor CORR over the HER, we plotted the scaling relations between ΔG_{*H} and ΔG_{*CHO} (Figure 2), and ΔG_{*H} and

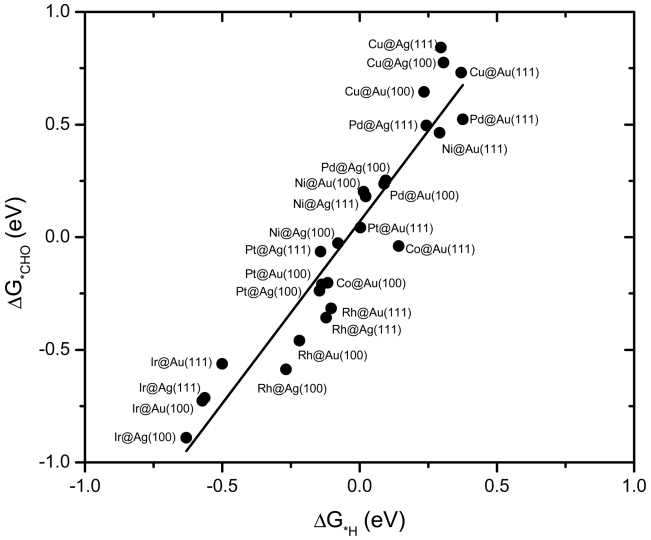

Figure 2. Gibbs free binding energy of *CHO (ΔG_{*CHO}) against that of *H (ΔG_{*H}). The equation for the linear fitting line is ΔG_{*CHO} = 1.61 × ΔG_{*H} + 0.07, and the correlation coefficient (R^2) is 0.90.

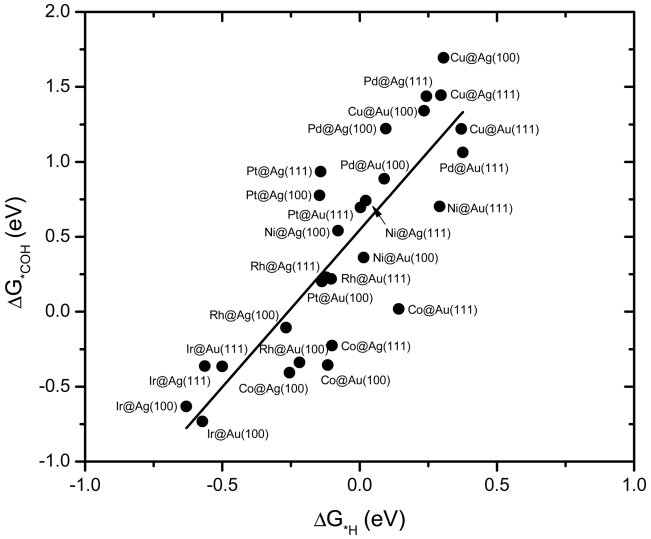

Figure 3. Gibbs free binding energy of *COH (ΔG_{*COH}) against that of *H (ΔG_{*H}). The equation for the linear fitting line is ΔG_{*COH} = 2.10 × ΔG_{*H} + 0.54, and R^2 = 0.71.

ΔG_{*COH} (Figure 3). Figures 2 and 3 show that the slopes for ΔG_{*CHO} vs ΔG_{*H} and ΔG_{*COH} vs ΔG_{*H} are 1.61 and 2.10, respectively. This indicates that when alloys bind strongly with H, they also bind with CHO and COH even more strongly, making CORR the major pathway. The larger slope for ΔG_{*COH} vs ΔG_{*H} (2.10), compared to that for ΔG_{*CHO} vs ΔG_{*H} (1.61), can be rationalized by the number of bonds formed between the COH and CHO and the surface: COH can form three bonds to the surface, while CHO can only form one.[55]

3.2. Mechanisms of CO Reduction to Methane Catalyzed by Rh@Au(100) and Rh@Ag(100).

Having identified several promising SAAs for CORR, we then selected two of them to study the reaction mechanism for further reduction of *CHO or *COH to C_1 products. Rh@Au(100) was chosen from the Au-based alloys for two reasons. First, Rh@Au(100) requires a smaller applied voltage for the reaction *CO → *CHO (−1.01 V vs RHE), which suggests that its energy consumption is less than the others. Second, *CHO on the surface of this catalyst is 0.24 eV more stable than *H, which guarantees that most of the electrical energy is directed to CORR, in preference to HER. From among the Ag-based SAAs, we chose Rh@Ag(100) for detailed mechanistic study, because *CHO for Rh@Ag(100) is 0.32 eV more stable than *H, guaranteeing selectivity for CORR over HER. In addition, although the required applied voltage for *CO → *CHO (−1.12 V_{RHE}) for Rh@Ag(100) is higher than that for Pt@Ag(100) (−0.83 V_{RHE}), the method to synthesize Rh@Ag is known.[56]

There are numerous possible CORR routes leading to the formation of either the 4 × (H^+ + e^-) reduction product, $CH_3OH_{(aq)}$, or the 6 × (H^+ + e^-) reduction product, $CH_{4(g)}$, from *CO, as depicted in Scheme 4. The first hydrogenation

Scheme 4. Schematic Description of Possible Reduction Pathways for the Surface-Bound CO (*CO)[a]

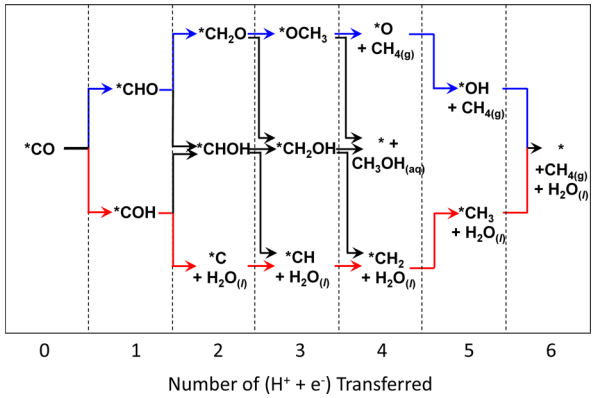

[a]Four-electron reduction of *CO leads to the formation of methanol, whereas six-electron reduction results in the formation of methane.

products are *CHO and *COH, while the second hydrogenation products are *CH_2O, *CHOH, and *C + $H_2O_{(l)}$, and the third hydrogenation products include *OCH_3, *CH_2OH, and *CH + $H_2O_{(l)}$. The fourth hydrogenation products are *O + $CH_{4(g)}$, *CH_3OH, and *CH_2 + $H_2O_{(l)}$, the fifth hydrogenation products are *OH + $CH_{4(g)}$, and *CH_3 + $H_2O_{(l)}$, and the sixth hydrogenation product is $CH_{4(g)}$ + $H_2O_{(l)}$. Desorption of surface-bound CH_3OH (*CH_3OH) results in the formation of $CH_3OH_{(aq)}$. In the absence of experimental information, we considered the thermodynamics for all possible pathways for Rh@Au(100) and Rh@Ag(100). However, the activation barrier for each elementary step was not determined.

Numerous DFT-based studies have been devoted to the investigation of the mechanisms of CO_2RR catalyzed by heterogeneous catalysts.[20,21,29,49,50,57−64] Since copper is the only material that can reduce CO_2RR to hydrocarbons with significant conversion,[26,65] most of the previous theretical studies have focused on the mechanism of CORR on Cu.[49,50,57] Two main pathways have emerged from these studies, differing

DOI: 10.1021/acscatal.6b01393
ACS Catal. 2016, 6, 7769−7777

primarily in the reaction intermediate formed by the reduction of *CO. Based on their investigation of CO_2RR catalyzed by the Cu(211) surface, Nørskov and co-workers proposed a reaction mechanism involving the following transformations:

$$*CO \rightarrow *CHO \rightarrow *CH_2O \rightarrow *OCH_3 \rightarrow *O + CH_{4(g)}$$
$$\rightarrow *OH + CH_{4(g)} \rightarrow * + CH_{4(g)} + H_2O_{(l)}$$

(colored blue in Scheme 4).[49] By contrast, based on their analysis of CORR on Cu(111), Janik and co-workers proposed that CH_4 involves the following transformations:

$$*CO \rightarrow *COH \rightarrow *C + H_2O_{(l)} \rightarrow *CH + H_2O_{(l)}$$
$$\rightarrow *CH_2 + H_2O_{(l)} \rightarrow *CH_3 + H_2O_{(l)} \rightarrow * + H_2O_{(l)} + CH_{4(g)}$$

(colored red in Scheme 4).[57] Recently, Goddard and co-workers have used implicit solvation plus applied electric voltage to revisit CO_2RR catalyzed by the Cu(111) surface.[50] They propose that the hydrogenation of *CO leads to the formation of *COH, in agreement with Janik;[57] however, the subsequent reduction of *COH leads to the formation of *CHOH, which is different from the pathways identified by Nørskov[49] and Janik.[57]

Our calculations show that along the most favorable pathway (Figure 4) for CORR catalyzed by Rh@Au(100), the first (H^+ + e^-) pair is added to the carbon of *CO to form *CHO, the second one is added to the oxygen to form *CHOH, and the third one is added to the oxygen to liberate $H_2O_{(l)}$, leading to the formation of *CH. (The free-energy surface for all possible reduction pathways can be found in Figure S1 in the Supporting Information). These steps are followed by further hydrogenation of *CH to *CH_2, *CH_3, and eventually to the formation of gaseous $CH_{4(g)}$ and the regeneration of the surface alloy site (*). For the *CO, *CHO, *CHOH, and *CH_3 intermediates, the adsorbates prefer to bind on the top site of Rh. However, *CHOH prefers to bind in the 4-fold hollow site formed by three Au and one Rh, and *CH_2 prefers to bind on the bridged site formed by Au and Rh. Analyzing the potential energy surface, we found that the most uphill step (the potential-determining step) is the initial reduction: *CO → *CHO with ΔG = 1.01 eV. Since each step involves only a single electron transfer, with an applied bias of −1.01 V_{RHE}, all the steps become downhill or thermoneutral.

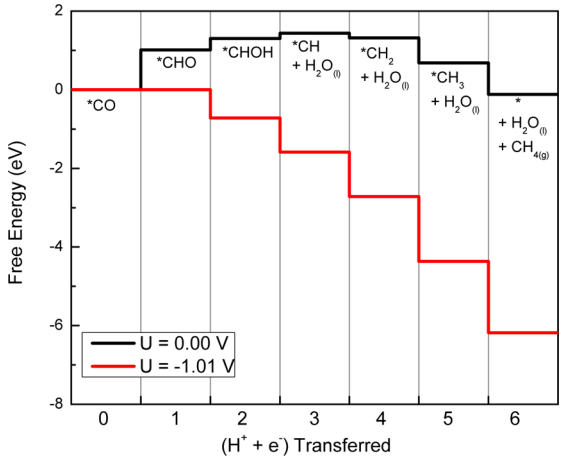

Figure 4. Gibbs free-energy diagram for *CO electrochemical reduction to methane catalyzed by Rh@Au(100) at 0.00 V_{RHE} (black) and −1.01 V_{RHE} (red). At −1.01 V_{RHE}, the free-energy change for each step is either zero or downhill.

In contrast, CORR catalyzed by Rh@Ag(100) takes a very different pathway, one that is similar to that proposed by Nørskov and co-workers (Figure 5).[49] The free-energy surface

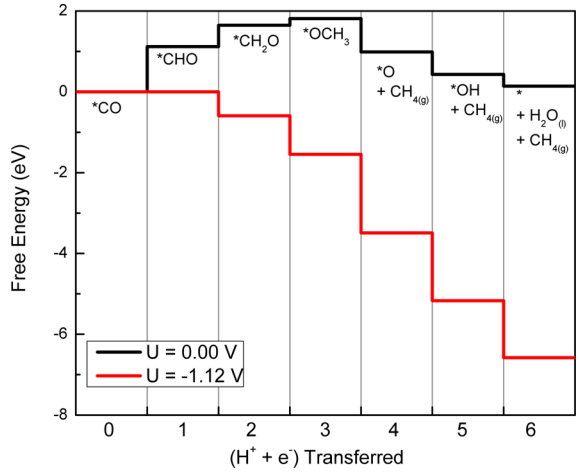

Figure 5. Gibbs free-energy diagram for *CO electrochemical reduction to methane catalyzed by Rh@Ag(100) at 0.00 V_{RHE} (black) and −1.12 V_{RHE} (red). At an applied bias of −1.12 V_{RHE}, the free-energy change for each step is either zero or downhill.

for all possible reduction pathways is detailed in Figure S2 in the Supporting Information. In the beginning, four (H^+ + e^-) pairs are successively added to the carbon of *CO to reduce it to *CHO, *CH_2O, *OCH_3, and then to * + free $CH_{4(g)}$. After those hydrogenation steps, a surface-bound oxygen (*O) is left behind, which is further reduced by two other (H^+ + e^-) pairs, first to form *OH, and then to liberate $H_2O_{(l)}$ and regenerate *. All of the adsorbates prefer to bind on the top site of Rh. From the calculated potential energy surface (PES), we found that the potential-determining step is *CO → *CHO with ΔG = 1.12 eV, and therefore, all the steps along the pathway become downhill or thermal neutral once a voltage of −1.12 V_{RHE} is applied.

3.3. Experimental Viability and Discussion. For the proposed M@Au (or Ag) SAAs, the single active site M is only involved in converting CO to C_1 products, while the surrounding Au or Ag reduces CO_2 and supplies CO for the M site. Therefore, another critical requirement for success of this type of one-pot tandem catalyst is whether the minimal electric voltage for CO reduction to $CH_{4(g)}$ or $CH_3OH_{(aq)}$ by M matches the voltage for efficient CO_2-to-CO reduction catalyzed by Au or Ag. If the minimum applied voltage required for the reduction CO to C_1 products is too high or too low, compared to the voltage for the maximum Faradaic efficiency for CO_2 reduction to CO, the SAAs will not be efficient and may not be selective for the CORR vs the HER.

For one of our proposed catalysts, Rh@Au(100), the minimum voltage needed to drive the CORR is −1.01 V_{RHE}. Experimental measurements show that, at this voltage, the Faradaic efficiency for CO_2 reduction to CO over Au is ~60%.[25] Assuming all CO produced by surrounding Au is reduced by M, then this means that only ~40% of the Faradaic efficiency is diverted to the HER. For Rh@Ag(100), the minimum bias needed to drive the CORR is −1.12 V_{RHE}, for which the Faradaic efficiency for CO_2 reduction to CO over Ag

DOI: 10.1021/acscatal.6b01393
ACS Catal. 2016, 6, 7769−7777

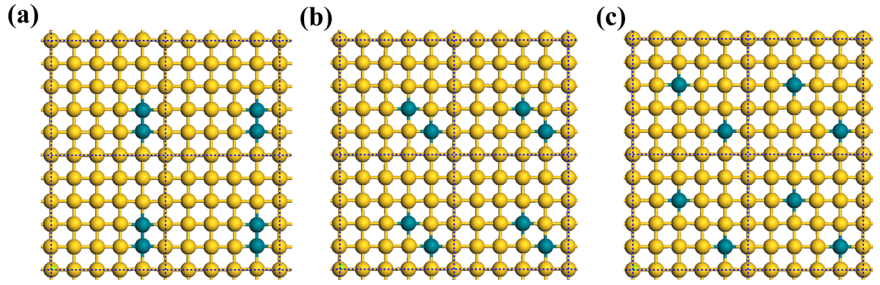

Figure 6. Configurations considered in evaluating the tendency of active sites toward island formation.

is as high as ~90%.[17] This suggests that the HER channel may consume as little as 10% of the Faradaic efficiency (assuming that the reduction of CO on M is 100% efficient). These results suggest that our proposed one-pot tandem SAA catalysts are potentially efficient for CO_2RR to CH_4. A critical issue remaining unanswered by the present work is whether or not the rate of CO conversion to CH_4 on the Rh sites embedded in the surface of Au or Ag is sufficiently active and sufficiently numerous to consume all, or a large fraction, of the CO generated on the host metal. To address this point, it will be necessary to determine the turnover frequencies (TOFs) for CO_2 reduction to CO on Au and Ag, as well as the TOF for CO conversion to CH_4. If the TOF for the latter reaction is sufficiently high, then it would be possible to achieve high overall Faradaic efficiencies for the reduction of CO_2 to CH_4 using Rh@Au or Rh@Ag catalysts.

Another important question about the viability of our proposed Rh@Au and Rh@Ag SAA catalysts is whether or not they can be synthesized and whether they would be stable. Rh and Au, and Rh and Ag are immiscible: while they can be mixed at high temperatures, phase separation occurs upon cooling.[66,67] However, recent advances in synthetic techniques have overcome this difficulty.[56,68,69] In particular, Humphrey and co-workers have discovered a microwave-assisted method that enables the synthesis of stable, homogeneous Rh@Au and Rh@Ag nanoparticles with broadly tunable Rh:Au and Rh:Ag ratios.[56]

Subsurface segregation of M is another problem, which may deactivate the proposed SAA catalysts. Co (2.522 J/m^2), Rh (2.659 J/m^2), and Ir (3.048 J/m^2) have larger surface free energies than Au (1.506 J/m^2) and Ag (1.246 J/m^2); therefore, they are likely to segregate into the subsurface under vacuum,[70,71] leading to an inactive catalyst. However, since it is well-known that CO binds with Co, Rh, and Ir more strongly than Au and Ag do (indeed, that is the basis of the usefulness of the SAAs for CORR), those Group 9 metals may prefer to be present on the surface under CO-rich conditions.[29] Indeed, Sansa et al. have used DFT to study CO-induced segregation in gold-based alloys, and they have predicted that, under CO environments, Co, Rh, and Ir will remain on the surface of Au(111) and Au(100).[72]

The aggregation of active sites into islands is another potential problem for the stability of SAAs. To test whether or not this is the case, additional calculations were performed for Rh@Au(100), one of the two most promising SAAs for CO_2RR. Rh@Au(100) was modeled by a three-layer 5 × 5 surface and the reciprocal space was sampled by a 2 × 2 × 1 Monkhorst-pack *k*-point net. During the geometry optimizations, the atoms in the bottom layer were fixed at their bulk positions, whereas the rest of atoms were allowed to relax. Two Au atoms on the top layer were replaced by Rh atoms, corresponding to an Rh surface concentration of 8%. Three surface configurations were considered: (a) two Rh atoms adjacent to each other along the *y*-axis, (b) two Rh atoms adjacent to each other along the *xy*-direction, and (c) two Rh atoms separated by Au atoms (see Figure 6). Our calculated results show that the three configurations are almost degenerate energetically, with configuration (c) being slightly more stable than configurations (a) and (b), by 0.01 and 0.02 eV, respectively. However, configuration (c) is expected to be more stable when entropy is taken into account. These results suggest that the proposed SAAs are stable to island formation.

Finally, it is appropriate to revisit some of the uncertainties in the computational protocol itself. For example, as discussed in the Computational Details of the Supporting Information, we observe an ~0.1 eV change in the difference in binding energy between H and CHO upon changing from a three-layer slab to a four-layer slab, as well as a similar shift upon increasing the slab thickness from three layers to four layers. While such shifts are not insignificant, they do not affect our main conclusions. The key point is that we find a free energy binding difference of nearly 0.4 eV in favor of CO_2RR over HER for the best single-atom alloys (e.g., Rh@Au(100)). This gap is large enough that potential errors on the order of 0.1 eV will not qualitatively change it, even if they lead directly to stabilization of the HER pathway (which, of course, is not clear). The same argument suggests that our main conclusions are likely to be robust to other possible errors imposed by computational limitations, such as deficiencies of the RPBE density functional itself.

4. CONCLUSIONS

Twenty-eight (28) single-atom alloys (SAAs) were studied and evaluated as catalysts for the CO_2 electrochemical reduction reaction to energy-rich hydrocarbons such as alkanes and alcohols in aqueous phase, using density functional theory (DFT) calculations together, with the Poisson−Boltzmann implicit solvation model. To be useful for the CO_2 reduction reaction (CO_2RR), the SAAs should contain isolated single-atom surface sites of M (M = Cu, Ni, Pd, Pt, Co, Rh, and Ir), as surface substitutions in Au or Ag. Initial reduction of CO_2 to CO occurs on the Au or Ag host, and CO then binds preferentially to M. We found that 14 SAAs favor the formation of *CHO or *COH over *H, which, for those systems, means that CO reduction is preferred over proton reduction. This suggests that, for these catalysts, CO_2 reduction is the major pathway, and the competitive evolution of hydrogen is suppressed. Most of the 14 promising SAAs contain M = Co, Rh, or Ir. This indicates that it is the identity of M rather than the surrounding metal that determines the performance of the SAA catalysts. The fact that M can bind only a single CO

DOI: 10.1021/acscatal.6b01393
ACS Catal. 2016, 6, 7769−7777

molecule also means that the SAAs will be selective for C_1 products, relative to larger hydrocarbons.

We also performed a detailed thermodynamic study of the reaction mechanism for two of the most promising SAAs: Rh@Au(100) and Rh@Ag(100). We found that both of these SAAs reduce CO_2 to methane, although the reduction occurs via different pathways. For Rh@Au(100), the reaction proceeds through the pathway

$$*CO \rightarrow *CHO \rightarrow *CHOH \rightarrow *CH + H_2O_{(l)} \rightarrow *CH_2 + H_2O_{(l)}$$
$$\rightarrow *CH_3 + H_2O_{(l)} \rightarrow * + H_2O_{(l)} + CH_{4(g)}$$

whereas, for Rh@Ag(100), it is

$$*CO \rightarrow *CHO \rightarrow *CH_2O \rightarrow *OCH_3 \rightarrow *O + CH_{4(g)}$$
$$\rightarrow *OH + CH_{4(g)} \rightarrow * + H_2O_{(l)} + CH_{4(g)}$$

The minimum applied voltages needed to drive the two electrocatalytic systems are −1.01 and −1.12 V_{RHE} for Rh@Au(100) and Rh@Ag(100), respectively, for which the Faradaic efficiencies for CO_2 reduction to CO are 60% for gold and 90% for silver. This suggests that SAA can efficiently reduce CO_2 to methane with as little as 40% Faradaic efficiency loss in the hydrogen evolution reaction for Rh@Au(100) and as little as 10% for Rh@Ag(100). We believe that this computational work provides encouraging motivation for experimental efforts to prepare and characterize SAAs for the electrochemical reduction of CO_2.

■ ASSOCIATED CONTENT

Supporting Information

The Supporting Information is available free of charge on the ACS Publications website at DOI: 10.1021/acscatal.6b01393.

Additional tables and details regarding computational methods (PDF)

■ AUTHOR INFORMATION

Corresponding Authors

*E-mail: alexbell@berkeley.edu (A. T. Bell).
*E-mail: mhg@cchem.berkeley.edu (M. Head-Gordon).

Notes

The authors declare no competing financial interest.

■ ACKNOWLEDGMENTS

This material is based on work performed in the Joint Center for Artificial Photosynthesis, a DOE Energy Innovation Hub, supported through the Office of Science of the U.S. Department of Energy, under Award No. DE-SC0004993.

■ REFERENCES

(1) Lewis, N. S.; Nocera, D. G. *Proc. Natl. Acad. Sci. U. S. A.* **2006**, *103*, 15729−15735.
(2) Cook, T. R.; Dogutan, D. K.; Reece, S. Y.; Surendranath, Y.; Teets, T. S.; Nocera, D. G. *Chem. Rev.* **2010**, *110*, 6474−6502.
(3) Thomas, C. D.; Cameron, A.; Green, R. E.; Bakkenes, M.; Beaumont, L. J.; Collingham, Y. C.; Erasmus, B. F. N.; de Siqueira, M. F.; Grainger, A.; Hannah, L.; Hughes, L.; Huntley, B.; van Jaarsveld, A. S.; Midgley, G. F.; Miles, L.; Ortega-Huerta, M. A.; Peterson, A. T.; Phillips, O. L.; Williams, S. E. *Nature* **2004**, *427*, 145−148.
(4) Rakowski Dubois, M.; Dubois, D. L. *Acc. Chem. Res.* **2009**, *42*, 1974−1982.
(5) Morris, A. J.; Meyer, G. J.; Fujita, E. *Acc. Chem. Res.* **2009**, *42*, 1983−1994.
(6) Appel, A. M.; Bercaw, J. E.; Bocarsly, A. B.; Dobbek, H.; DuBois, D. L.; Dupuis, M.; Ferry, J. G.; Fujita, E.; Hille, R.; Kenis, P. J. A.; Kerfeld, C. A.; Morris, R. H.; Peden, C. H. F.; Portis, A. R.; Ragsdale, S. W.; Rauchfuss, T. B.; Reek, J. N. H.; Seefeldt, L. C.; Thauer, R. K.; Waldrop, G. L. *Chem. Rev.* **2013**, *113*, 6621−6658.
(7) White, J. L.; Baruch, M. F.; Pander, J. E., III; Hu, Y.; Fortmeyer, I. C.; Park, J. E.; Zhang, T.; Liao, K.; Gu, J.; Yan, Y.; Shaw, T. W.; Abelev, E.; Bocarsly, A. B. *Chem. Rev.* **2015**, *115*, 12888−12935.
(8) Qiao, J. L.; Liu, Y. Y.; Hong, F.; Zhang, J. J. *Chem. Soc. Rev.* **2014**, *43*, 631−675.
(9) Li, C. W.; Ciston, J.; Kanan, M. W. *Nature* **2014**, *508*, 504−507.
(10) Schouten, K. J. P.; Qin, Z. S.; Gallent, E. P.; Koper, M. T. M. *J. Am. Chem. Soc.* **2012**, *134*, 9864−9867.
(11) Schouten, K. J. P.; Kwon, Y.; van der Ham, C. J. M.; Qin, Z.; Koper, M. T. M. *Chem. Sci.* **2011**, *2*, 1902−1909.
(12) Jedidi, A.; Rasul, S.; Masih, D.; Cavallo, L.; Takanabe, K. *J. Mater. Chem. A* **2015**, *3*, 19085−19092.
(13) Rasul, S.; Anjum, D. H.; Jedidi, A.; Minenkov, Y.; Cavallo, L.; Takanabe, K. *Angew. Chem., Int. Ed.* **2015**, *54*, 2146−2150.
(14) Elgrishi, N.; Chambers, M. B.; Fontecave, M. *Chem. Sci.* **2015**, *6*, 2522−2531.
(15) Zhang, Y. J.; Sethuraman, V.; Michalsky, R.; Peterson, A. A. *ACS Catal.* **2014**, *4*, 3742−3748.
(16) Li, C. W.; Kanan, M. W. *J. Am. Chem. Soc.* **2012**, *134*, 7231−7234.
(17) Hatsukade, T.; Kuhl, K. P.; Cave, E. R.; Abram, D. N.; Jaramillo, T. F. *Phys. Chem. Chem. Phys.* **2014**, *16*, 13814−13819.
(18) Kim, D.; Resasco, J.; Yu, Y.; Asiri, A. M.; Yang, P. D. *Nat. Commun.* **2014**, *5*, 4948.
(19) Cheng, M. J.; Kwon, Y.; Head-Gordon, M.; Bell, A. T. *J. Phys. Chem. C* **2015**, *119*, 21345−21352.
(20) Karamad, M.; Tripkovic, V.; Rossmeisl, J. *ACS Catal.* **2014**, *4*, 2268−2273.
(21) Tripkovic, V.; Vanin, M.; Karamad, M.; Björketun, M. E.; Jacobsen, K. W.; Thygesen, K. S.; Rossmeisl, J. *J. Phys. Chem. C* **2013**, *117*, 9187−9195.
(22) Rossmeisl, J.; Logadottir, A.; Norskov, J. K. *Chem. Phys.* **2005**, *319*, 178−184.
(23) Carrasquillo-Flores, R.; Ro, I.; Kumbhalkar, M. D.; Burt, S.; Carrero, C. A.; Alba-Rubio, A. C.; Miller, J. T.; Hermans, I.; Huber, G. W.; Dumesic, J. A. *J. Am. Chem. Soc.* **2015**, *137*, 10317−10325.
(24) Lu, Q.; Rosen, J.; Zhou, Y.; Hutchings, G. S.; Kimmel, Y. C.; Chen, J. G. G.; Jiao, F. *Nat. Commun.* **2014**, *5*, 3242.
(25) Hahn, C.; Abram, D. N.; Hansen, H. A.; Hatsukade, T.; Jackson, A.; Johnson, N. C.; Hellstern, T. R.; Kuhl, K. P.; Cave, E. R.; Feaster, J. T.; Jaramillo, T. F. *J. Mater. Chem. A* **2015**, *3*, 20185−20194.
(26) Hori, Y.; Wakebe, H.; Tsukamoto, T.; Koga, O. *Electrochim. Acta* **1994**, *39*, 1833−1839.
(27) Chen, Y. H.; Li, C. W.; Kanan, M. W. *J. Am. Chem. Soc.* **2012**, *134*, 19969−19972.
(28) Zhu, W. L.; Michalsky, R.; Metin, O.; Lv, H. F.; Guo, S. J.; Wright, C. J.; Sun, X. L.; Peterson, A. A.; Sun, S. H. *J. Am. Chem. Soc.* **2013**, *135*, 16833−16836.
(29) Peterson, A. A.; Norskov, J. K. *J. Phys. Chem. Lett.* **2012**, *3*, 251−258.
(30) Lucci, F. R.; Lawton, T. J.; Pronschinske, A.; Sykes, E. C. H. *J. Phys. Chem. C* **2014**, *118*, 3015−3022.
(31) Lucci, F. R.; Marcinkowski, M. D.; Lawton, T. J.; Sykes, E. C. H. *J. Phys. Chem. C* **2015**, *119*, 24351−24357.
(32) Pei, G. X.; Liu, X. Y.; Wang, A. Q.; Li, L.; Huang, Y. Q.; Zhang, T.; Lee, J. W.; Jang, B. W. L.; Mou, C. Y. *New J. Chem.* **2014**, *38*, 2043−2051.
(33) Pei, G. X.; Liu, X. Y.; Wang, A. Q.; Lee, A. F.; Isaacs, M. A.; Li, L.; Pan, X. L.; Yang, X. F.; Wang, X. D.; Tai, Z. J.; Wilson, K.; Zhang, T. *ACS Catal.* **2015**, *5*, 3717−3725.
(34) Lucci, F. R.; Liu, J. L.; Marcinkowski, M. D.; Yang, M.; Allard, L. F.; Flytzani-Stephanopoulos, M.; Sykes, E. C. H. *Nat. Commun.* **2015**, *6*, 8550.

DOI: 10.1021/acscatal.6b01393
ACS Catal. 2016, 6, 7769−7777

(35) Boucher, M. B.; Zugic, B.; Cladaras, G.; Kammert, J.; Marcinkowski, M. D.; Lawton, T. J.; Sykes, E. C. H.; Flytzani-Stephanopoulos, M. *Phys. Chem. Chem. Phys.* **2013**, *15*, 12187−12196.
(36) Kyriakou, G.; Boucher, M. B.; Jewell, A. D.; Lewis, E. A.; Lawton, T. J.; Baber, A. E.; Tierney, H. L.; Flytzani-Stephanopoulos, M.; Sykes, E. C. H. *Science* **2012**, *335*, 1209−1212.
(37) Zhang, L.; Wang, A.; Miller, J. T.; Liu, X.; Yang, X.; Wang, W.; Li, L.; Huang, Y.; Mou, C. Y.; Zhang, T. *ACS Catal.* **2014**, *4*, 1546−1553.
(38) Jirkovsky, J. S.; Panas, I.; Ahlberg, E.; Halasa, M.; Romani, S.; Schiffrin, D. J. *J. Am. Chem. Soc.* **2011**, *133*, 19432−19441.
(39) Aich, P.; Wei, H. J.; Basan, B.; Kropf, A. J.; Schweitzer, N. M.; Marshall, C. L.; Miller, J. T.; Meyer, R. *J. Phys. Chem. C* **2015**, *119*, 18140−18148.
(40) Hammer, B.; Hansen, L. B.; Norskov, J. K. *Phys. Rev. B: Condens. Matter Mater. Phys.* **1999**, *59*, 7413−7421.
(41) Blochl, P. E. *Phys. Rev. B: Condens. Matter Mater. Phys.* **1994**, *50*, 17953−17979.
(42) Kresse, G.; Joubert, D. *Phys. Rev. B: Condens. Matter Mater. Phys.* **1999**, *59*, 1758−1775.
(43) Kresse, G.; Furthmuller, J. *Phys. Rev. B: Condens. Matter Mater. Phys.* **1996**, *54*, 11169−11186.
(44) Kresse, G.; Furthmuller, J. *Comput. Mater. Sci.* **1996**, *6*, 15−50.
(45) Kresse, G.; Hafner, J. *Phys. Rev. B: Condens. Matter Mater. Phys.* **1993**, *47*, 558−561.
(46) Kresse, G.; Hafner, J. *Phys. Rev. B: Condens. Matter Mater. Phys.* **1994**, *49*, 14251−14269.
(47) Mathew, K.; Hennig, R. G. *ArXiv* **2016**, 1601.03346.
(48) Blaylock, D. W.; Ogura, T.; Green, W. H.; Beran, G. J. O. *J. Phys. Chem. C* **2009**, *113*, 4898−4908.
(49) Peterson, A. A.; Abild-Pedersen, F.; Studt, F.; Rossmeisl, J.; Norskov, J. K. *Energy Environ. Sci.* **2010**, *3*, 1311−1315.
(50) Xiao, H.; Cheng, T.; Goddard, W. A.; Sundararaman, R. *J. Am. Chem. Soc.* **2016**, *138*, 483−486.
(51) Nørskov, J. K.; Rossmeisl, J.; Logadottir, A.; Lindqvist, L.; Kitchin, J. R.; Bligaard, T.; Jonsson, H. *J. Phys. Chem. B* **2004**, *108*, 17886−17892.
(52) Oloman, C.; Li, H. *ChemSusChem* **2008**, *1*, 385−391.
(53) Steinmann, S. N.; Michel, C.; Schwiedernoch, R.; Sautet, P. *Phys. Chem. Chem. Phys.* **2015**, *17*, 13949−13963.
(54) Steinmann, S. N.; Michel, C.; Schwiedernoch, R.; Filhol, J. S.; Sautet, P. *ChemPhysChem* **2015**, *16*, 2307−2311.
(55) Abild-Pedersen, F.; Greeley, J.; Studt, F.; Rossmeisl, J.; Munter, T. R.; Moses, P. G.; Skulason, E.; Bligaard, T.; Norskov, J. K. *Phys. Rev. Lett.* **2007**, *99*, 016105.
(56) Garcia, S.; Zhang, L.; Piburn, G. W.; Henkelman, G.; Humphrey, S. M. *ACS Nano* **2014**, *8*, 11512−11521.
(57) Nie, X. W.; Esopi, M. R.; Janik, M. J.; Asthagiri, A. *Angew. Chem., Int. Ed.* **2013**, *52*, 2459−2462.
(58) Back, S.; Kim, H.; Jung, Y. *ACS Catal.* **2015**, *5*, 965−971.
(59) Shi, C.; O'Grady, C. P.; Peterson, A. A.; Hansen, H. A.; Norskov, J. K. *Phys. Chem. Chem. Phys.* **2013**, *15*, 7114−7122.
(60) Luo, W. J.; Nie, X. W.; Janik, M. J.; Asthagiri, A. *ACS Catal.* **2016**, *6*, 219−229.
(61) Karamad, M.; Hansen, H. A.; Rossmeisl, J.; Norskov, J. K. *ACS Catal.* **2015**, *5*, 4075−4081.
(62) Hirunsit, P.; Soodsawang, W.; Limtrakul, J. *J. Phys. Chem. C* **2015**, *119*, 8238−8249.
(63) Lim, H. K.; Shin, H.; Goddard, W. A.; Hwang, Y. J.; Min, B. K.; Kim, H. *J. Am. Chem. Soc.* **2014**, *136*, 11355−11361.
(64) Bernstein, N. J.; Akhade, S. A.; Janik, M. J. *Phys. Chem. Chem. Phys.* **2014**, *16*, 13708−13717.
(65) Kuhl, K. P.; Hatsukade, T.; Cave, E. R.; Abram, D. N.; Kibsgaard, J.; Jaramillo, T. F. *J. Am. Chem. Soc.* **2014**, *136*, 14107−14113.
(66) Zarkevich, N. A.; Tan, T. L.; Johnson, D. D. *Phys. Rev. B* **2007**, *75*, 104203.
(67) Davies, R. H.; Dinsdale, A. T.; Gisby, J. A.; Robinson, J. A. J.; Martin, S. M. *CALPHAD: Comput. Coupling Phase Diagrams Thermochem.* **2002**, *26*, 229−271.
(68) Essinger-Hileman, E. R.; DeCicco, D.; Bondi, J. F.; Schaak, R. E. *J. Mater. Chem.* **2011**, *21*, 11599−11604.
(69) Kusada, K.; Yamauchi, M.; Kobayashi, H.; Kitagawa, H.; Kubota, Y. *J. Am. Chem. Soc.* **2010**, *132*, 15896−15898.
(70) Tyson, W. R.; Miller, W. A. *Surf. Sci.* **1977**, *62*, 267−276.
(71) Vitos, L.; Ruban, A. V.; Skriver, H. L.; Kollar, J. *Surf. Sci.* **1998**, *411*, 186−202.
(72) Sansa, M.; Dhouib, A.; Guesmi, H. *J. Chem. Phys.* **2014**, *141*, 064709.

DOI: 10.1021/acscatal.6b01393
ACS Catal. 2016, 6, 7769−7777